The Scientific Journal of Cihan University – Sulaimaniya **PP: 10-29**
Volume (5), Issue (2), December 2021
ISSN 2520-7377 (Online), ISSN 2520-5102 (Print)

COVID-19 Infection Detection from Chest X-Ray Images Using Feature Fusion and Machine Learning

Faraidoon Hassan Ahmad[1], Shakhawan Hares Wady[2]

[1] Department of Pharmacognosy and Pharmaceutical Chemistry, College of Pharmacy, University of Sulaimani, Sulaimani, Iraq
[2]Applied Computer, College of Medicals and Applied Sciences, Charmo University, Chamchamal, Sulaimani, Iraq
[1,2] Department of Information Technology, University College of Goizha, Sulaimani, Iraq

Email: Faraidoon.Ahmad@univsul.edu.iq[1] ,Shakhawan.hares@charmouniversity.edu.iq[2]

Abstract:

COVID-19 is a severe viral infection that poses a serious threat on humanity as a whole; it has affected almost all aspects of life. To overcome the threat, experts use different methods to detect the infection of COVID-19. One of the main techniques is the use of medical images which provides experts with valuable information to accurately detect the infection. Many researches have concentrated on automation of COVID-19 classification using artificial intelligence techniques on chest X-ray (CXR) images. This paper concentrated on designing and developing an intelligent pipeline for the COVID-19 identification by fusing the features extracted using Curvelet Transform (CT), Gabor Wavelet Transform (GWT), and Local Gradient Increasing Pattern (LGIP), then to classify the CXR images, the images were fed into four machine learning classifiers, Discriminant Analysis (DISC), Ensemble, Random Forest (RF), and Support Vector Machine (SVM). To verify the validity of the proposed model performance, a total of 7232 CXR healthy and COVID-19 images were used which were obtained from a COVID-19 Radiography database. Experimental results indicated that the proposed feature fusion technique assured a satisfactory performance in terms of identifying COVID-19 compared to other state-of-the-art works with overall testing accuracy of 96.18%, precision of 95.46%, sensitivity of 96.98%, and F1-score of 96.21% using SVM classifier.

Keywords: COVID-19 diagnosis, Chest X-rays, Feature Extraction, Machine learning.

الملخص:

كوفيد-١٩ هي عدوى فيروسية شديدة و تشكل تهديدا لصحة و حياة الأنسان. استخدام الصور الطبية يزود الخبراء بمعلومات مفيدة. بحوث عديدة ركزت على صور اشعة الصدر بأستخدام تقنيات الذكاء الصناعي لتحديد الأصابة بكوفيد-١٩ اوتوماتيكيا. هذا البحث صممت و طورت نظام ذكي لتحديد الأصابة بكوفيد-١٩ بدمج الميزات المستخلصة من Curvelet Transform (CT) و Gabor Wavelet Transform(GWT) و Local Gradient Increasing Pattern (LGIP) و ارسالها الى مصنفات اليات التعلم Discriminant Analysis (DISC) و Ensemble و Random Forest (RF) و Support Vector Machine(SVM) لتصنيف صور اشعة الصدر. للتحقق من كفائة النظام, ٧٢٣٢ صورة لأشعة الصدر تم استخدامها, توزعت الى صنفين: اعتيادى (صحي) و كوفيد-١٩، الصور مأخوذة من قاعدة البيانات راديوكرافي. النتائج المختبرية اظهرت تفوق النظام و اداء مميز في تصنيف كوفيد-١٩ مقارنة بالنظم الحديثة المماثلة حيث أن معدل الدقة وصلت الى (٩٦،١٨٪) ودرجة احكام (٩٥،٤٦) و درجة الحساسية (٩٦،٩٨٪) و F1-score هي (٩٦،٢١٪) و بأستخدام مصنف SVM.

DOI: http://dx.doi.org/10.25098/5.2.16

The Scientific Journal of Cihan University – Sulaimaniya **PP: 10-29**
Volume (5), Issue (2), December 2021
ISSN 2520-7377 (Online), ISSN 2520-5102 (Print)

الكلمات المفتاحية: تشخيص كوفيد-١٩، اشعة الصدر، استخراج المميزات، اليات التعلم.

پوختە:

نەخۆشی کۆرۆنا (کۆڤید-١٩) یەکێکە لە نەخۆشیە ڤایرۆسیە گواستراوەکان کە دەبێتە هۆی زنجیرەیەک زیان بە تەندروستی و ژیانی مرۆڤەکان. بەکارهێنانی وێنەی پزیشکی کاری پسپۆرەکان بەرەو پێشتر دەبات بەهۆی زانیاریيە گرنگەکانی ناوی. توێژینەوەی زۆر لەسەر وێنەی تیشکی سنگ کراوە بە بەکارهێنانی تەکنیکەکانی زیرەکی دەستکرد بۆ دیاریکردنی توشبوون بە پەتای کۆڤید-١٩. لەم توێژینەوەیەدا سیستمێکی زیرەکی پێشکەوتوو دیزاین کراوە بۆ دیاریکردنی توشبوون بە کۆڤید-١٩ بە لێکدانی ئەو فیچەرانەی کە دەستمان دەکەوێت بە بەکارهێنانی Curvelet Transform (CT) و Gabor Wavelet Transform(GWT) و Local Gradient Increasing Pattern (LGIP) کە دەنێردرێن بۆ ئامرازە فێرکارییەکانی Discriminant Analysis (DISC) و Ensemble و Random Forest (RF) و Support Vector Machine(SVM). بۆ تاقیکردنەوەی کارایی سیستمەکە (٧٢٣٢) وێنەی تیشکی بەکارهاتووە، کە پۆلێن کراوە بۆ هەردوو حاڵەتی ئاسایی (تەندروست) و کۆڤید-١٩، کە لە داتابەیسی کۆڤید-١٩ ڕادیۆگرافی وەرگیراون. ئەنجامە تاقیگەییەکان دەرخەری ئەوەن کە ئەم سیستمە داهێنراوە بە تەکنیکی لێکدانی فیچەرەکان تا ئاستێکی باش سەرکەوتووە بۆ دیاریکردنی توشبوون بە کۆڤید-١٩ بە بەراورد بە سیستمەکانی دیکە کە تێکڕای کارایيەکەی دەگاتە (٩٦،١٨٪)، بە تۆکمەیی (٩٥،٤٦٪) وە هەستیاری (٩٦،٩٨٪) و وە F1-score (٩٦،٢١٪) بە بەکارهێنانی SVM.

کلیلە ووشەکان: دیاریکردنی کۆڤید-١٩، تیشکی سنگ، دەرهێنانی فیچەر، ئامرازەکانی فێرکردن.

1. Introduction

COVID-19 (coronavirus disease 2019) is an infectious disease caused by the coronavirus strain, Severe Acute Respiratory Syndrome Coronavirus 2 (SARS-CoV-2). On March 11, 2020, the World Health Organization (WHO) declared the disease to be a pandemic. Given the recent increase in new COVID-19 cases and the resumption of daily activities around the world, the need to control the pandemic should be emphasized even more [1]. Early diagnosis and separation of infected patients are a key factor to increase the chances of successful treatment for infected patients and minimizes the risk of an infectious disease like COVID-19 spreading in the community [2]. Several screenings are used to detect the onset symptoms of the COVID-19 virus [3], including the Reverse Transcriptase-polymerase Chain Reaction (RT-PCR). Radiographical images such as CXR or Computed Tomography (CT) are a technique of routine diagnosis for lung-related conditions, such as pneumonia [4] and tuberculosis (TB) [5] which can also be used in the detection of COVID-19. In addition, medical images of the infected COVID-19 patients and Artificial Intelligence (AI) were found valuable for rapid evaluation of these patients. Therefore, the design and implementation of AI image classification tools for COVID-19 with limited data over a short time period was an urgent requirement to combat the present pandemic [6]. Studies using chest X-rays to diagnose COVID-19 have binary or multiple categories. Some researches rely on raw data, while others employ a feature extraction method [7].

Section 2 puts forward a literature review. Section 3 presents a complete examination of the proposed workflow, including sections such as an overview of system architecture, COVID-19 dataset, data preprocessing, feature extractors, feature fusion and classification, and performance metrics. Section 4 discusses the results attained after applying different feature extractors and comparing them with the recommended approaches. Lastly, Section 5 provides the conclusion of the work.

DOI: http://dx.doi.org/10.25098/5.2.16

The Scientific Journal of Cihan University – Sulaimaniya **PP: 10-29**
Volume (5), Issue (2), December 2021
ISSN 2520-7377 (Online), ISSN 2520-5102 (Print)

2. Related Literature

In biomedical image analysis and processing, machine learning and image processing approaches have yielded outstanding results, particularly in the field of chest radiology. These methods are often used in the classification of pulmonary tuberculosis and the detection of lung nodules. For automatic classification of these disease-causing infections, a number of approaches have been successfully applied. Different methodologies include CNNs, ensemble learning, feature extraction, and feature selection, among others [8]. Recently, a number of works were performed with the help of various AI-based techniques to detect COVID-19 using X-ray images. To increase system performance in classifying COVID-19, normal, and other lung disorders, various transfer learning approaches, different system designs, and ensemble solutions were proposed [9]. A short review of some significant contributions from the existing literature is provided.

Based on chest X-ray images, Tuan D. Pham [1] intended to develop a deep learning model that is capable of detecting COVID-19 cases more precisely. In this work, AlexNet, GoogleNet, and SqueezeNet, three pretrained CNNs, were chosen and fine-tuned without data augmentation to perform 2-class and 3-class classification tasks utilizing three public CXR datasets. A novel hybrid multi-modal deep learning technique was proposed by [10] to support expert radiologists in rapid and accurate interpretation of the images for identifying the COVID-19 virus in CXR images. In numerous state-of-the-art deep learning models such as baseline ResNet, Inception-v3, Inception ResNet-v2, DenseNet169, and NASNetLarge. Narinder Singh Punn and Sonali Agarwal [11] introduced the random oversampling and weighted class loss function strategy for unbiased fine-tuned learning to conduct binary (as normal and COVID-19 conditions) and multi-class (as COVID-19, pneumonia, and normal conditions) classification of posteroanterior CXR images. The authors in [12] proposed an effective machine learning classification which precisely distinguished images of COVID-19 CXR from ordinary cases and pneumonia caused by other viruses. Features were extracted using both the spatial domain (Texture, GLDM, and GLCM) and frequency domain (Wavelet and FFT), and they achieved the highest classification accuracy and sensitivity result to distinguish COVID-19 cases from non-COVID-19 cases. López-Cabrera's study [13] suggested some of the challenges of using artificial intelligence approaches into the automatic COVID-19 categorization in the present scientific literature. It has been recommended that in most of the reviewed works an incorrect evaluation protocol is applied, which leads to overestimating the outcomes.

In [14], for the detection of coronavirus pneumonia infected patients utilizing CXR radiographs, five pre-trained convolutional neural network-based models (ResNet50, ResNet101, ResNet152, InceptionV3 and Inception-ResNetV2) have been proposed. The study [15] proposed a COVID-19 infection detection pipeline based on CXR images. The relevant features from the CXR images were extracted and picked using the Hybrid Social Group Optimization (HSGO) method. Using a variety of classifiers, the selected features were then utilized to classify the CXR images. In an attempt to classify Covid-19 affected patients using their CXR scans, the authors in [16] experimented different CNN models, including Inception V3, Xception, and ResNeXt. 6432 CXR scan samples were collected from the Kaggle repository to analyze the model's performance, with 5467 images being used for training and 965 for validation. In [17], the authors addressed a novel CNN framework and

DOI: http://dx.doi.org/10.25098/5.2.16

The Scientific Journal of Cihan University – Sulaimaniya **PP: 10-29**
Volume (5), Issue (2), December 2021
ISSN 2520-7377 (Online), ISSN 2520-5102 (Print)

a network learning methodology for categorizing COVID-19 from CXR images, CNN learns robust features by mixing channel-shuffling and using two residual skip connections. It also utilizes dual branching in combination with many convolutional layers to generate a variety of contextual features. In [18], the authors developed utilizing machine vision to diagnose COVID-19 from CXR images. Through CNN training, the features extracted from X-ray images by the Histogram Oriented Gradient (HOG) and Convolutional Neural Network (CNN) were combined to construct the classification model (VGGNet). For enhanced edge preservation and lower noise in the images, the Modified Anisotropic Diffusion Filtering (MADF) technique was used. The substantial fracture region in the raw X-ray images was identified using a watershed segmentation approach. The study [19] proposed a novel statistical workflow through the purely Bayesian learning approach based on the shifted scaled mixture design Dirichlet in order to discrimination toward patients who are either negative or positive with certain viruses and pneumonia. In another work [20] the authors proposed an automatic detection framework for COVID-19 infection based on CXR images using transfer learning concept. Zulfaezal and his colleagues [21] developed a deep learning technique to detect COVID-19 cases based on ResNet-101 convolutional neural network procedure.

The authors in [22] proposed a deep learning classification model for detection of coronavirus using X-ray images based on deep features and SVM classifier. The research paper [23] built a deep learning classifier based on an ensemble of pre-trained deep neural networks (DNNS), specifically, ReNet34, ReNet50¸ ReNet152, and vgg16 for detecting patients' positive for COVID-19. In [24], the authors addressed a method for visual diagnosis of cases of COVID-19 on CXR images. This proposed extraction of COVID-19 x-ray images was carried out at one fractional moment (i.e., FrMEMs). An amended version of Manta Ray Foraging Optimization (MRFO) for selecting the relevant features and KNN classifier to determine if a CXR image is a COVID-19 or a normal case were utilized. The study [25] investigated the potentials of automatic corona virus diagnostics machine learning methods from CXR images using Logistic Regression (LR) and CNN classifiers. To distinguish COVID-19 patients from bacterial pneumonia, viral pneumonia, and normal cases. The authors in [26] utilized a deep CNN-based technique with transfer learning. They used nine pre-trained CNN prototypes to investigate transfer learning strategies, concluding that fine-tuning the pre-trained CNN models could be successfully applied to a limited class dataset. Al-antari et al. [27] recommended a simultaneous deep learning CAD framework based on the YOLO predictor to detect and diagnose COVID-19, differentiating it from eight other respiratory diseases: atelectasis, infiltration, pneumothorax, masses, effusion, pneumonia, cardiomegaly, and nodules. Afifi and his colleagues [28] developed a set of deep learning models using global and local attention -based features for the detection of COVID-19 on CXR images. The study [19] proposed one-shot cluster-based method for efficient classification of COVID-19 CXR images as it classifies images of four classes, viz., pneumonia bacterial, pneumonia virus, normal, and COVID-19.

This paper discusses and presents an improved form of LBP, called Local Gradient Increasing Pattern (LGIP) along with CT and GWT for feature extraction. A balanced and large dataset with 3616 CXR images in each of two classes was used as training data. Thus, a proposed model was constructed by applying fusion strategy that can be used to detect and diagnose cases of COVID-19 on CXR images.

DOI: http://dx.doi.org/10.25098/5.2.16

The Scientific Journal of Cihan University – Sulaimaniya **PP: 10-29**
Volume (5), Issue (2), December 2021
ISSN 2520-7377 (Online), ISSN 2520-5102 (Print)

3. Proposed Methodology

3.1 System Architecture

To detect COVID-19, the proposed approach used X-ray scans as input data. To begin, this method transformed RGB images to grayscale and defined the Region of Interest (ROI) by removing unwanted areas. Furthermore, the system examined three feature extractors: CT, GWT, and LGIP. First, a feature vector was extracted from the X-ray COVID-19 Radiography Database using the CT approach. Then the GWT and LGIP techniques were performed to extract another two feature vectors from the same X-ray images. These three features were fused and fed into the classification model as input data. The number of features extracted by one method was insufficient to accurately identify COVID-19. However, using three distinct strategies to extract features could lead to a large number of features for accurate classification. In this case, fusion was considered as a concatenation of the three distinct vectors. Finally, the fused features were then classified X-ray images to determine if they were COVID-19 or not using four well-known classifiers (DISC, Ensemble, RF, and SVM). The key steps of the proposed system design were shown in Figure 1.

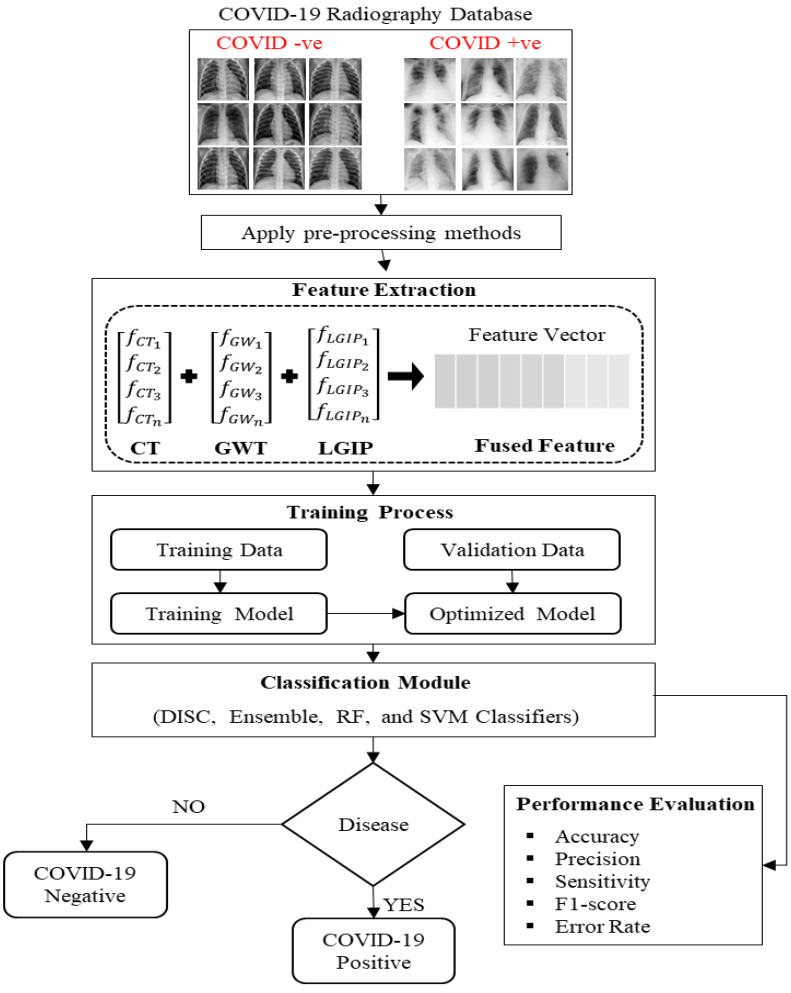

Figure 1: Workflow of proposed system

DOI: http://dx.doi.org/10.25098/5.2.16

The Scientific Journal of Cihan University – Sulaimaniya **PP: 10-29**
Volume (5), Issue (2), December 2021
ISSN 2520-7377 (Online), ISSN 2520-5102 (Print)

3.2 COVID-19 Dataset

The patients' CXR images were collected and kept in a common place. As a benchmark for evaluating the intelligence system's performance, the images were classified as COVID-19-positive or COVID-19-negative. In this study, COVID-19 Radiography database [29,30], which is a public database of COVID-19 CXR, was used to validate the system's performance. The COVID-19 Radiography database consists of CXR of 3616 COVID-19 positive cases along with 10,192 Normal, 6012 Lung Opacity (Non-COVID lung infection), and 1345 Viral Pneumonia images. In this study, a constructed balanced dataset of 7232 images (3616 normal and 3616 COVID-19 positive) were randomly selected from this database for a two-class classification. In Figure 2, representative CXR images of normal (healthy) and COVID-19 patients are given, respectively.

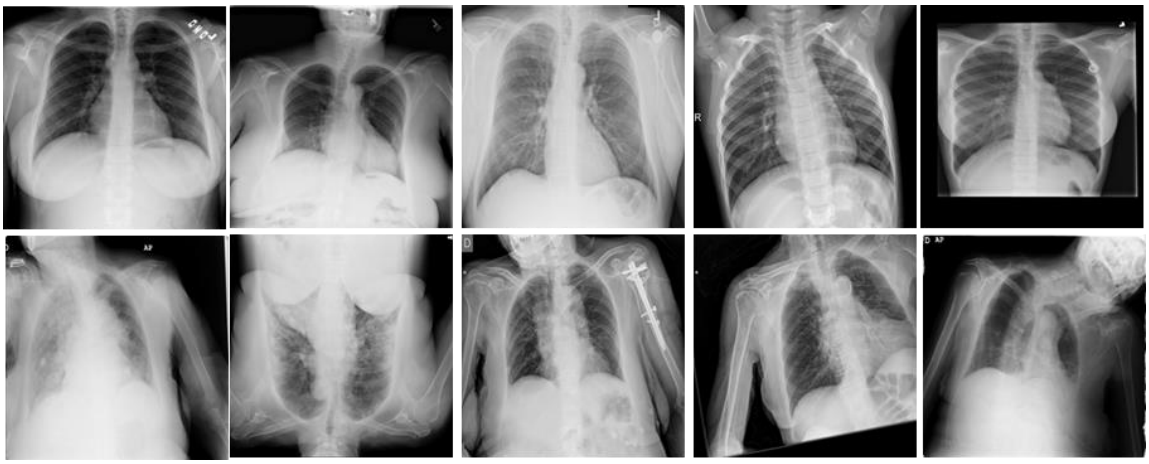

Figure 2: Representative CXR images of normal (healthy) (first row) and images of COVID-19 affected cases (second row) patients

3.3 Data Pre-processing

Image processing is a significant stage to accomplish meaningful information and accurate classification by removing noisy or unwanted pixels from each image. To remove superfluous text and machine annotation around images, the ROI was localized (see Figure 3), cropped and resized images to 512x512 pixels after the input images were converted from RGB to grayscale (see Figure 4). The ROI on the CXR images was determined by an area covering mainly lung region in order to achieve valuable information. As the raw images were taken in real life with a large variance in exposure and contrast, image enhancement was needed for superior classification performance. Therefore, the contrast enhancement of grayscale images was implemented using Contrast Limited Adaptive Histogram Equalization technique (CLAHE) and the median filter for a proper brightness and enhancement. Before importing the input CXR images into a feature extraction task, image adjustment was performed to improve the quality of images as shown in Figure (5).

DOI: http://dx.doi.org/10.25098/5.2.16

The Scientific Journal of Cihan University – Sulaimaniya **PP: 10-29**
Volume (5), Issue (2), December 2021
ISSN 2520-7377 (Online), ISSN 2520-5102 (Print)

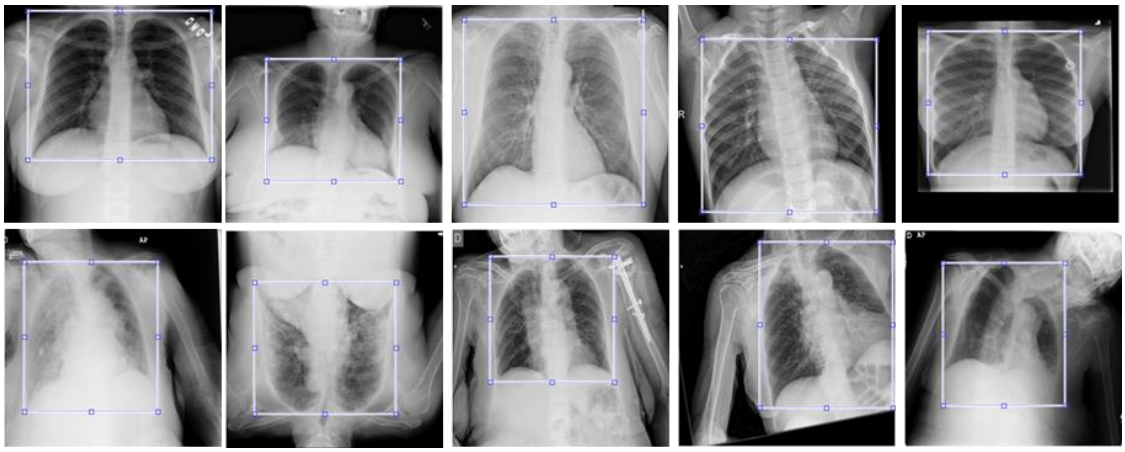

Figure 3: Samples of CXR images dataset used for proposed system; a) localized ROI area of healthy individuals (first row), b) localized ROI area of COVID-19 affected cases (second row).

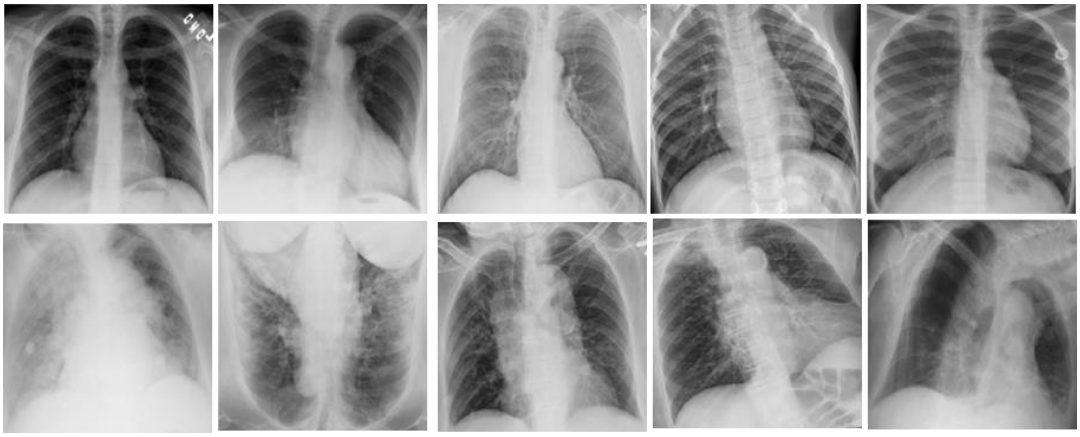

Figure 4: Samples of CXR images dataset used for proposed system; a) cropped ROI area of healthy individuals (first row), b) cropped ROI area of COVID-19 affected cases (second row).

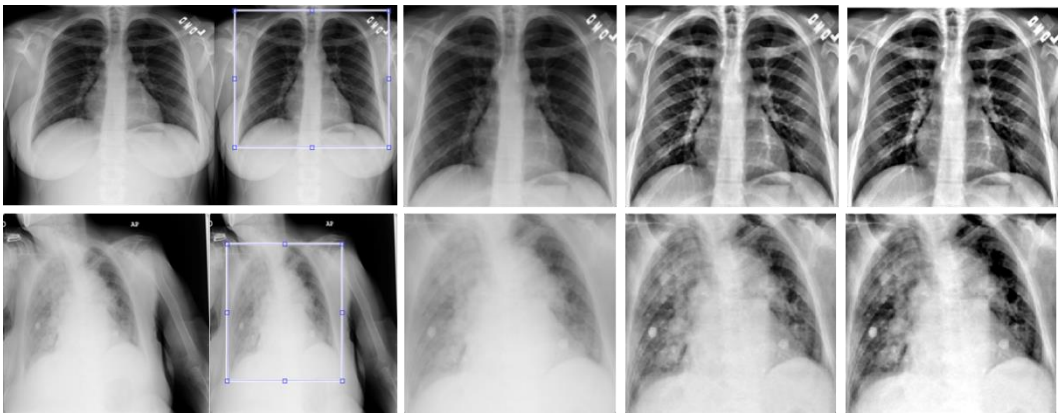

(a) (b) (c) (d) (e)

Figure 5: Samples of CXR images dataset used for proposed system; a) original CXR image, b) localized ROI area, c) resized ROI area, d) denoised CXR image, e) adjusted CXR image.

DOI: http://dx.doi.org/10.25098/5.2.16

The Scientific Journal of Cihan University – Sulaimaniya **PP: 10-29**
Volume (5), Issue (2), December 2021
ISSN 2520-7377 (Online), ISSN 2520-5102 (Print)

3.4 Feature Extraction

Feature extraction is the process of transforming the raw pixel values from an image into a set of features, normally this stage involves obtaining important features extracted from input patterns that can be used in the classification tasks [31]. Three sets of extracted features (CL, GWT, and LGIP) are included for feature extraction in the proposed scheme.

3.4.1 Discrete Curvelet Transform

The Curvelet transform is a new anisotropic directional wavelet transform that allows for optimal object sparse representation. Candès et al. [32] introduced two novel Curvelet transforms based on various Fourier operations in 2005, namely, unequally spaced fast Fourier transform (USFFT) and wrapping based fast CT, which are simpler, faster, and less redundant than prior techniques. CT based on wrapping of Fourier samples takes an image having dimension M x N as input in the form of a Cartesian array $f[x,y]$ such that $0 \le x < M, 0 \le y < N$ and creates a number of Curvelet coefficients indexed by j scale , θ orientation and two spatial location parameters of curvelets (K_1, K_2) as output [33].

$$CT(j,\theta,K_1,K_2) = \sum_{\substack{0\le x<M \\ 0\le y<N}} f[x,y]\,.\,\varphi_{j,\theta,K_1,K_2}[x,y] \qquad (1)$$

Wrapping-based CT is a multiscale transform that has a pyramid structure with numerous orientations at each scale. In the frequency domain, this pyramid structure is made up of numerous sub bands of different scales. Curvelet transforms are widely used in the frequency domain to reach higher levels of efficiency. That is, both the Curvelet and the image are converted in the Fourier frequency domain and then multiplied. Finally, the Curvelet coefficients are obtained by inverse Fourier transformation of the product Therefore, above equation can be written in frequency domain as [33],

$$CT = IFFT\,\{\,FFT(Curvelet)\;x\;FFT(image)\} \qquad (2)$$

CT scan depict an image in a variety of scales, each with a different number of orientations. In this study, CT was applied to an image to obtain its coefficients and these coefficients were then used to form the texture descriptor of that image. Once the curvelet coefficients were generated and stored in each subband, the mean and standard deviation of the coefficients associated with each subband were computed. A set of 52 features for each image was extracted from the dataset of CXR images at the end of this extraction process.

3.4.2 Gabor Wavelet Transform

Gabor-wavelets are used to capture the image's local structure, which includes spatial frequency (scales), spatial localization, and orientation selectivity. As a result, Gabor-wavelets are widely used in a variety of disciplines, including texture analysis and image segmentation [34]. A two-dimensional Gabor filter is a Gaussian kernel function modulated by a complex sinusoidal plane wave in the spatial domain, defined as,

DOI: http://dx.doi.org/10.25098/5.2.16

The Scientific Journal of Cihan University – Sulaimaniya **PP: 10-29**
Volume (5), Issue (2), December 2021
ISSN 2520-7377 (Online), ISSN 2520-5102 (Print)

$$F(u_1, u_2) = \exp\left(-\frac{(\hat{u}_1{}^2 + \gamma^2 \hat{u}_2{}^2)}{2\sigma^2}\right) x\ cos\left(\frac{2\pi}{\lambda}\hat{u}_1\right), \quad (3)$$

$$\hat{u}_1 = u_1 cos\theta + u_2 sin\theta \quad (4)$$

$$\hat{u}_2 = -u_1 sin\theta + u_2 cos\theta \quad (5)$$

Where the arguments $\hat{u}_1$ and $\hat{u}_2$ specify the position of a light impulse in the visual field, θ is the orientation of the normal to the parallel stripes of a Gabor function, σ is the standard deviation of the Gaussian envelope and λ is the spatial aspect ratio which specifies the ellipticity of the support of the Gabor function. In this work, Gabor wavelets filters in four different scales and six orientations were used and a set of 48 features for each image was extracted from the dataset of CXR images.

3.4.3 Local Gradient Increasing Pattern (LGIP)

LGIP is a pixel-based binary imaging descriptor that is robust against to fluctuations in illumination and white noise. Consequently, it's employed to make the binary vectors for the vertical and horizontal sub-image feature matrices that arise from partial image division [35]. LGIP is used to represent the magnitude and direction of an increasing trend in local intensity. First, LGIP calculates gradient responses in eight possible orientations at each pixel using Sobel masks [36] $M_0, M_1 \dots\dots, M_7$ as shown in Figure 6. Depending on the sign of the gradient value, each mask's gradient value is encoded into a single bit (1 or 0). As a result, each pixel in the partial CXR image has an 8-bit code descriptor. These eight masks are applied on each pixel. If the mask is positive for the pixel response, then the resulting bit is set to 1, or 0. Therefore for every pixel, a value of 8 bit is generated, where a given bit is the corresponding result of a particular mask. Alternatively, like the LBP operator, the eight bits can be determined using intensity comparisons between the core pixel and its neighbors to speed up calculation. In this work, the Sobel gradient operator was used to boost stability in the presence of non-uniform light variations and random noise and finally a set of 37 features for each image was extracted from the dataset of CXR images.

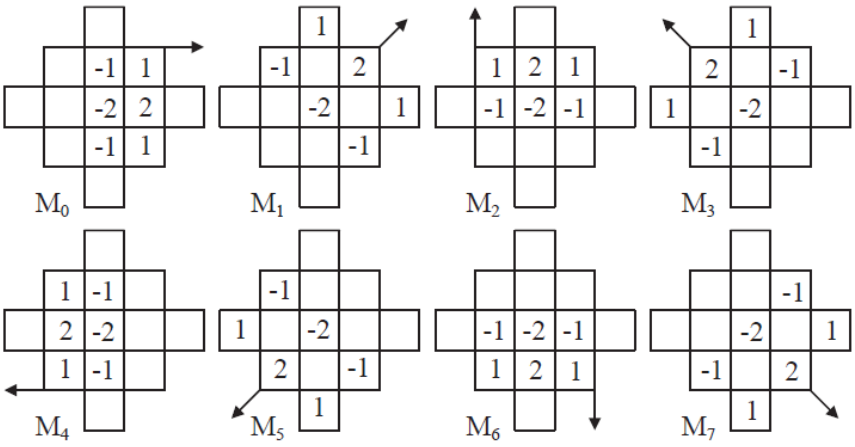

Figure 6: Sobel gradient masks in eight orientations [36].

DOI: http://dx.doi.org/10.25098/5.2.16

The Scientific Journal of Cihan University – Sulaimaniya **PP: 10-29**
Volume (5), Issue (2), December 2021
ISSN 2520-7377 (Online), ISSN 2520-5102 (Print)

3.5 Feature Fusion and Classification

Data fusion has been applied in several applications for machine learning and computer vision. Feature fusion, in particular, can combine multiple feature vectors. The multi-feature fusion can improve the robustness of the model predictions [37]. This work proposed a fusion of feature vectors attained by a combination of CT (1 x 52), GWT (1x 48), and LGIP (1 x 37) methods. Equations (6), (7), and (8) represent features extracted by CT, GWT, and LGIP, respectively. The extracted feature vectors were combined by concatenation and represented by Equation (9).

$$F_{CT_{1\,x\,n}} = \{CT_{1\,x\,1} + CT_{1\,x\,2} + CT_{1\,x\,3} \ldots\ldots\ldots CT_{1\,x\,n}\} \quad (6)$$

$$F_{GW_{1\,x\,m}} = \{GW_{1\,x\,1} + GW_{1\,x\,2} + GW_{1\,x\,3} \ldots\ldots\ldots GW_{1\,x\,m}\} \quad (7)$$

$$F_{LGIP_{1\,x\,k}} = \{LGIP_{1\,x\,1} + LGIP_{1\,x\,2} + LGIP_{1\,x\,3} \ldots\ldots\ldots LGIP_{1\,x\,k}\} \quad (8)$$

$$Fused\ (Features\ vector)_{1\,x\,p}^{cat} = \{F_{CT_{1\,x\,n}}, F_{GW_{1\,x\,m}}, F_{LGIP_{1\,x\,k}}\} \quad (9)$$

Then the features extracted by CT, GWT, and LGIP were fused with 137 features. This fusion vector, which considered as the final input for the training and testing dataset, was fed to the classifiers in order to validate the proposed approach and identify COVID-19 images. In the proposed workflow, machine learning models were used to identify patients affected by COVID-19 infection. To achieve the objective of identifying COVID-19 positive patients among normal healthy individuals', four pattern recognition classifiers namely DISC, Ensemble, RF, and SVM classifiers were separately performed.

3.6 Evaluations metrics

For COVID-19 classification from CXR images, four widely used performance metrics were utilized to evaluate the proposed model's performance: accuracy, sensitivity, precision, and F1-score. To compute the metrics specified by Equations (10)– (13), four distinct performance parameters were used: true-positive (TP), true-negative (TN), false-positive (FP), and false-negative (FN).

$$Accuracy = \frac{TP + TN}{TP + TN + FP + FN} \quad (10)$$

$$Sensitivity = \frac{TN}{TN + FP} \quad (11)$$

$$Precision = \frac{TP}{TP + FP} \quad (12)$$

$$F1 - score = \frac{2 * Precision * Sensitivity}{Precision + Sensitivity} \quad (13)$$

DOI: http://dx.doi.org/10.25098/5.2.16

The Scientific Journal of Cihan University – Sulaimaniya **PP: 10-29**
Volume (5), Issue (2), December 2021
ISSN 2520-7377 (Online), ISSN 2520-5102 (Print)

4. Result and Discussion

The performance of the proposed model was evaluated based on extracted features derived from CL, GWT, and LGIP coefficients for more than 7200 CXR images to automatically identify the class of the input image. All experiments were conducted in MATLAB using CXR images described in Section 3.2. Different scenarios using different features individually and different combinations of CL, GWT, and LGIP features have been suggested. For each scenario, these extracted features were classified by using four pattern recognition classifiers (i.e., DISC, Ensemble, RF, and SVM) to see which scenario could perform better classification performance. Furthermore, the entire dataset was divided into two groups: 80% for training the model and 20% for evaluation of the classification performance using holdout cross-validation technique. Performances of the suggested scenarios were analyzed through a number of different measures including accuracy, sensitivity, precision, F1-score, and error rate computed from confusion matrix.

From the experiments performed on self-collected dataset, the detailed category/class wise analysis of each scenario was evaluated in terms of accuracy and overall accuracy as (mean ± SD) with DISC (Table 1), Ensemble (Table 2), RF (Table 3), and SVM (Table 4) classifiers respectively. Among these scenarios in Table 1 and as depicted in Table 4, it is concluded that combining the CL, GWT, and LGIP features (scenario 7) together attain the highest overall accuracy of 92.35 ± 0.50 % and 96.18 ± 0.43 % followed by fusion of GL and GWT features (scenario 4) with 90.32 ± 0.50 % and 95.02 ± 0.59 % along with DISC and SVM classifiers respectively, while the classification overall accuracy of features derived from LGIP method had the lowest scoring (84.00 ± 0.85 % and 91.07 ± 0.87). In the case of Ensemble (Table 2) and RF (Table 3) classifiers use, it can be observed that the highest classification overall accuracy of 92.78 ± 0.52 % and 91.05 ± 0.86 % were achieved along with combining features extracted from the CL (52 features), GWT (37 features), and LGIP (40 features) methods, whereas GWT method gave the lowest performance results recording 87.88 ± 0.80 % and 85.47 ± 0.72 % overall accuracy respectively as compared to the other scenarios.

TABLE 1: Performance analysis on overall accuracy with DISC classifier. The highlighted accuracy in bold indicates the best classification result.

Methods	Features	Per Class Accuracy (%)		Overall Accuracy (%)
		Non-COVID	COVID	
CT	52	88.45 ± 1.03	82.37 ± 1.57	85.41 ± 1.07
GWT	48	82.69 ± 1.53	87.64 ± 0.86	85.17 ± 0.81
LGIP	37	83.49 ± 1.32	84.50 ± 0.89	84.00 ± 0.85
CT + GWT	100	91.17 ± 1.37	89.47 ± 0.92	90.32 ± 0.58
CT + LGIP	89	91.03 ± 1.15	89.36 ± 1.38	90.20 ± 0.75
GWT+ LGIP	85	88.02 ± 1.34	90.06 ± 1.00	89.04 ± 0.58
CT + GWT + LGIP	137	**93.31 ± 0.36**	**91.38 ± 0.91**	**92.35 ± 0.50**

DOI: http://dx.doi.org/10.25098/5.2.16

The Scientific Journal of Cihan University – Sulaimaniya **PP: 10-29**
Volume (5), Issue (2), December 2021
ISSN 2520-7377 (Online), ISSN 2520-5102 (Print)

TABLE 2: Performance analysis on overall accuracy with Ensemble classifier. The highlighted accuracy in bold indicates the best classification result.

Methods	Features	Per Class Accuracy (%)		Overall Accuracy (%)
		Non-COVID	COVID	
CT	52	91.03 ± 1.24	89.79 ± 1.17	90.41 ± 0.73
GWT	48	85.53 ± 1.31	90.23 ± 0.56	87.88 ± 0.80
LGIP	37	85.08 ± 1.42	91.25 ± 1.17	88.17 ± 1.00
CT + GWT	100	92.11 ± 0.92	93.09 ± 1.08	92.6 ± 0.76
CT + LGIP	89	92.82 ± 1.23	92.33 ± 1.10	92.57 ± 0.65
GWT+ LGIP	85	88.63 ± 1.36	92.73 ± 1.06	90.68 ± 0.91
CT + GWT + LGIP	137	**92.15 ± 1.15**	**93.41 ± 0.69**	**92.78 ± 0.52**

TABLE 3: Performance analysis on overall accuracy with Random Forest classifier. The highlighted accuracy in bold indicates the best classification result.

Methods	Features	Per Class Accuracy (%)		Overall Accuracy (%)
		Non-COVID	COVID	
CT	52	90.41 ± 1.01	86.00 ± 0.73	88.20 ± 0.57
GWT	48	85.72 ± 1.00	85.21 ± 0.92	85.47 ± 0.72
LGIP	37	85.14 ± 1.33	85.85 ± 0.89	85.49 ± 0.79
CT + GWT	100	91.56 ± 1.08	89.14 ± 0.8	90.35 ± 0.67
CT + LGIP	89	92.19 ± 1.09	88.96 ± 0.69	90.58 ± 0.48
GWT+ LGIP	85	88.07 ± 1.29	87.44 ± 1.47	87.75 ± 0.73
CT + GWT + LGIP	137	**92.71 ± 1.19**	**89.4 ± 1.16**	**91.05 ± 0.86**

TABLE 4: Performance analysis on overall accuracy with SVM classifier. The highlighted accuracy in bold indicates the best classification result.

Methods	Features	Per Class Accuracy (%)		Overall Accuracy (%)
		Non-COVID	COVID	
CT	52	93.7 ± 1.38	91.63 ± 0.89	92.66 ± 0.74
GWT	48	92.78 ± 0.94	91.39 ± 0.82	92.08 ± 0.58
LGIP	37	91.36 ± 1.57	90.78 ± 0.98	91.07 ± 0.89
CT + GWT	100	95.71 ± 0.65	94.34 ± 1.06	95.02 ± 0.59
CT + LGIP	89	96.04 ± 0.63	93.96 ± 0.63	95.00 ± 0.55
GWT+ LGIP	85	94.31 ± 0.95	93.30 ± 0.71	93.81 ± 0.60
CT + GWT + LGIP	137	**96.98 ± 0.63**	**95.38 ± 0.69**	**96.18 ± 0.43**

Based on the experimental results for all seven scenarios presented in Figure 7, it can be concluded that the fusion of features extracted from CL, GWT, and LGIP techniques has a positive impact on the performance and outperformed the other scenarios. The results revealed that all four classifiers achieved the highest overall accuracy of 96.18 ± 0.43 %, 92.78 ± 0.52 %, 92.35 ± 0.50 %, and 91.05

DOI: http://dx.doi.org/10.25098/5.2.16

The Scientific Journal of Cihan University – Sulaimaniya **PP: 10-29**
Volume (5), Issue (2), December 2021
ISSN 2520-7377 (Online), ISSN 2520-5102 (Print)

± 0.86 % by using SVM, Ensemble, DISC and RF classifiers respectively. On the other hand, the fusion of CL, GWT, and LGIP techniques with SVM classifier was sufficient to record maximal overall accuracy performance of 96.18 ± 0.43 % among the remaining classifiers for all scenarios.

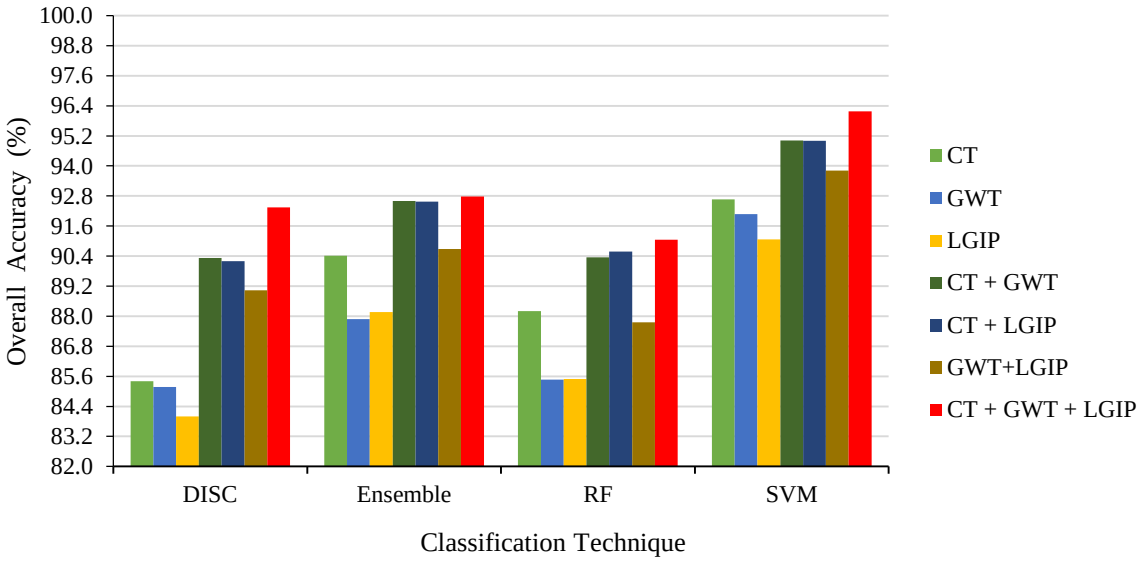

Figure 7: Comparison of overall accuracies for different scenarios using different classifiers.

The same fact has been concluded by investigating other performance measures (precision, recall, and F1-score) to evaluate the proposed model. For all classifiers, the best precision rate was achieved with a set of features fusion of CL, GWT and LGIP methods (scenario 7) which outperformed the other scenarios. The results of scenario 7 provided that all four classifiers attained the peak precision of 95.46%, 93.34%, 91.55%, and 89.75% using SVM, Ensemble, DISC and RF classifiers respectively; however, the lowest precision rate of 83.40 % was recorded using Curvelet method with DISC classifier. Moreover, the experiment recorded maximum precision performance of 95.46% with SVM classifier among the remaining classifiers for all scenarios. Comparison results of precision rates of all system scenarios with SVM, DISC, Ensemble and RF classifiers are presented in Figure 8.

DOI: http://dx.doi.org/10.25098/5.2.16

The Scientific Journal of Cihan University – Sulaimaniya **PP: 10-29**
Volume (5), Issue (2), December 2021
ISSN 2520-7377 (Online), ISSN 2520-5102 (Print)

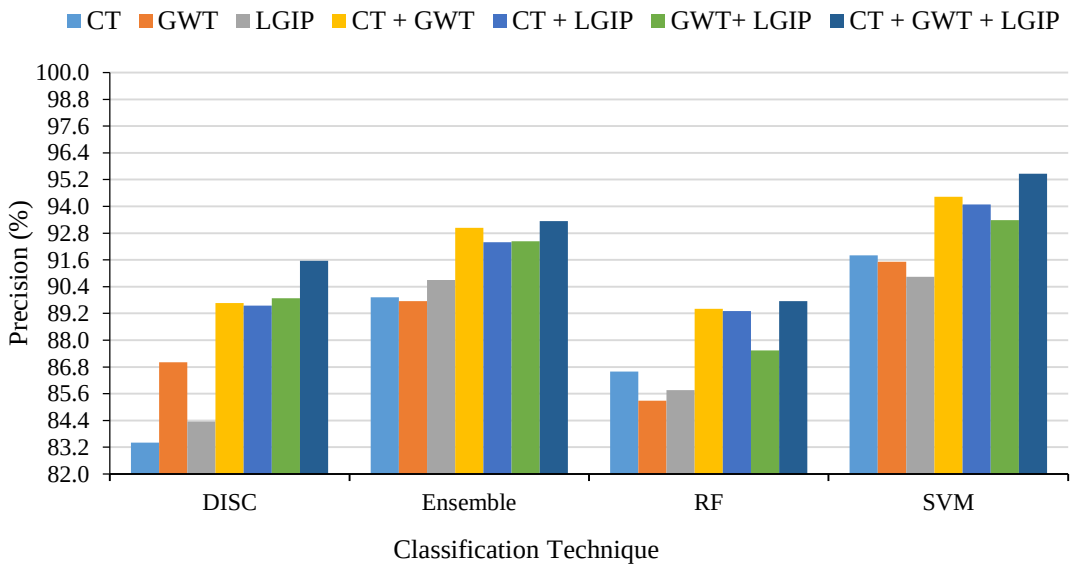

Figure 8: Comparison of precision for different scenarios using different classifiers.

Furthermore, the fusion of features from CL, GWT and LGIP methods outperformed the others in terms of sensitivity rates as 96.98%, 93.32%, 92.71%, and 92.16% were achieved using SVM, DISC, RF and Ensemble classifiers respectively (Figure 9); conversely, the lowest sensitivity rate of 82.70 % has been recorded when GWT method was utilized with DISC classifier. Based on the experimental results for all four classifiers depicted in Figure 9, it can be verified that the value of sensitivity rate with SVM classifier was overall superior and outperformed the other classifiers. With regard to the F1-score rates, the results presented in Figure 10 demonstrate the superiority of the fusion of CL, GWT and LGIP scenario and undoubtedly it yielded excellent results which defiantly go beyond the other scenarios. The best performance with F1-score rate of 96.21% was achieved using fusion of CL, GWT and LGIP methods with SVM classifier, which surpassed other classifiers with F1-scor rates of 92.74%, 92.43%, and 91.20% for Ensemble, DISC, and RF classifiers respectively; however, the F1-score rate of LGIP method using DISC classifier had the lowest recording of 83.92 %.

DOI: http://dx.doi.org/10.25098/5.2.16

The Scientific Journal of Cihan University – Sulaimaniya **PP: 10-29**
Volume (5), Issue (2), December 2021
ISSN 2520-7377 (Online), ISSN 2520-5102 (Print)

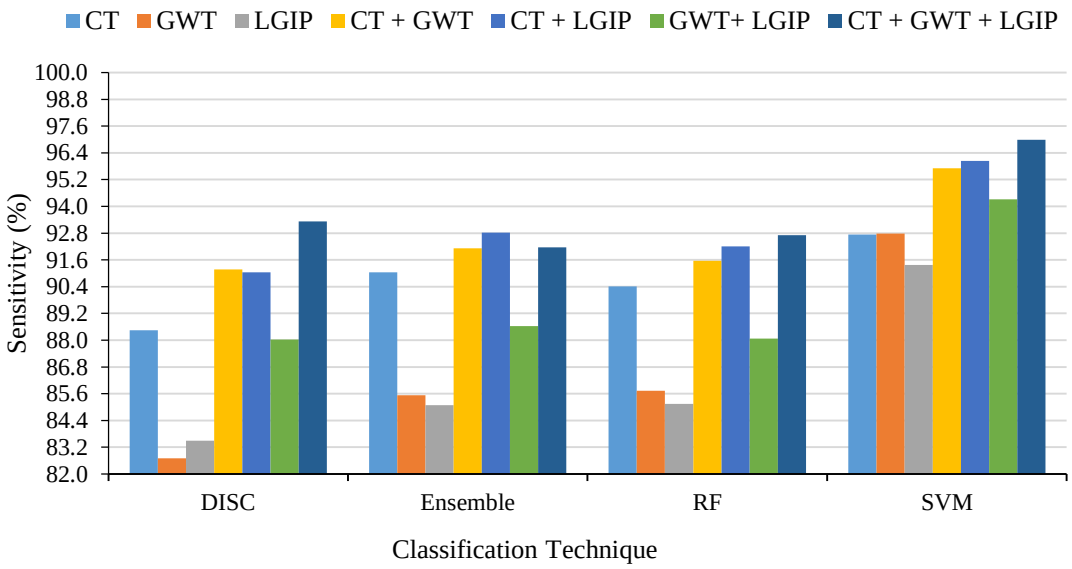

Figure 9: Comparison of sensitivity for different scenarios using different classifiers.

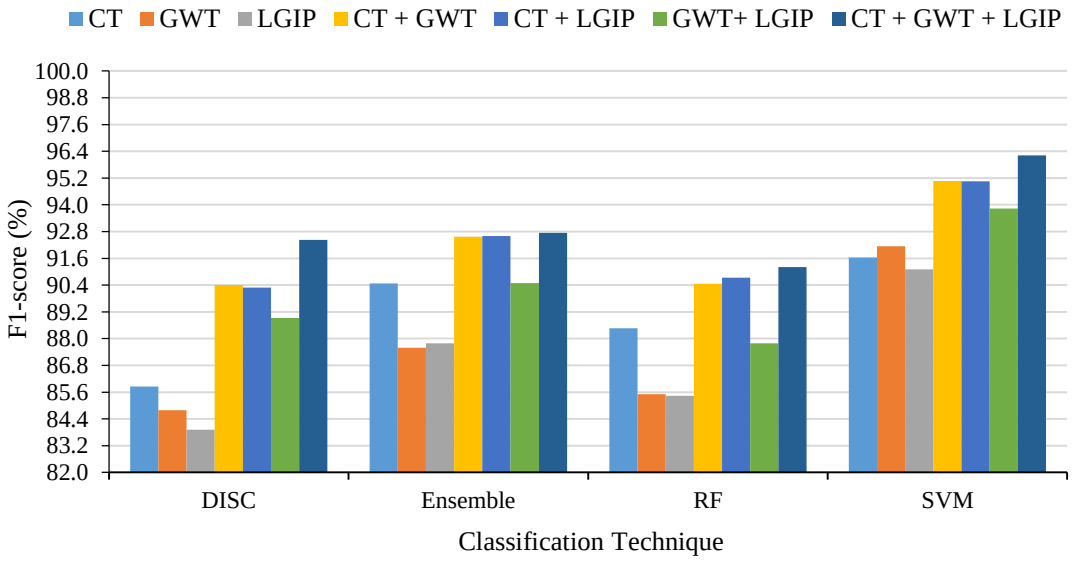

Figure 10: Comparison of F1-score for different scenarios using different classifiers.

Moreover, the experiments from (Figure 11) clearly demonstrated that the features derived by fusion of CR, GWT and LGIP scenario outperformed other scenarios and recorded the highest precision, sensitivity, and F1-score rates with SVM classifier. Considering the obtained results, the highest precision, sensitivity, and F1-score scores of the features extracted using fused CR, GWT and LGIP methods were 96.21%, 96.98, and 95.46% respectively, and was achieved using 137 effective features. While, the lowest precision, sensitivity, and F1-score scores were attained with a score of 91.10%, 91.37, and 90.85% respectively, and was achieved using 40 extracted features.

DOI: http://dx.doi.org/10.25098/5.2.16

The Scientific Journal of Cihan University – Sulaimaniya **PP: 10-29**
Volume (5), Issue (2), December 2021
ISSN 2520-7377 (Online), ISSN 2520-5102 (Print)

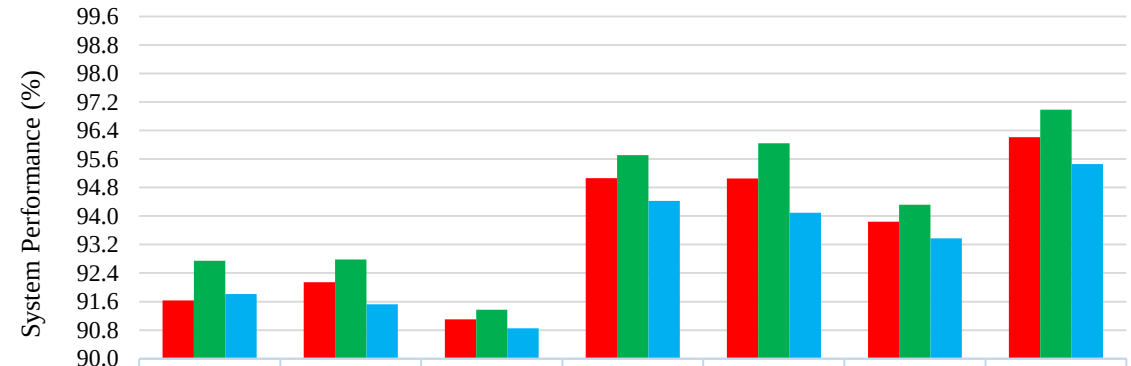

	CT	GWT	LGIP	CT + GWT	CT + LGIP	GWT+LGIP	CT + GWT + LGIP
Precision	91.63	92.14	91.10	95.06	95.06	93.84	96.21
Sensitivity	92.74	92.78	91.37	95.71	96.04	94.32	96.98
F1-score	91.81	91.52	90.85	94.43	94.09	93.38	95.46

Figure 11: Comparison of system performance for different scenarios using SVM classifier.

In this study, the performances of the suggested scenarios were also analyzed through misclassification error rate metric using the same dataset and computing environment. As demonstrated by (Figure 12), the misclassification error rates for the suggested scenarios were measured. The findings verify that the fusion of CR, GWT and LGIP scenario results in a lower misclassification error of 3.82% rate which confirms that the proposed scenario performs considerably much better than other suggesting scenarios. Therefore, this scenario was chosen as a proposed method for detecting and diagnosing cases of COVID-19 on CXR images.

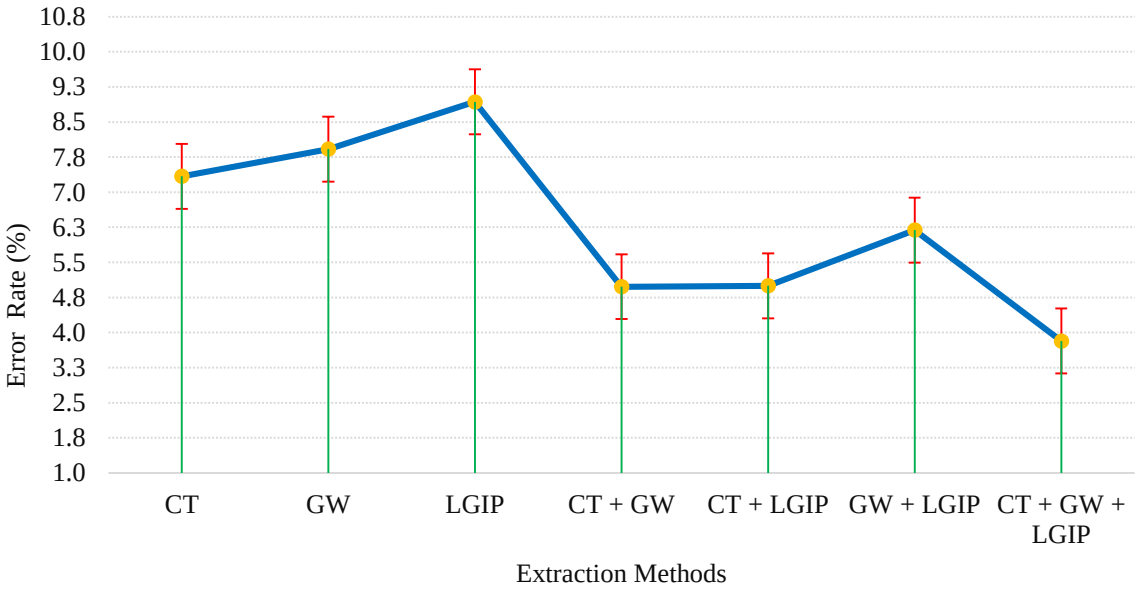

Figure 12: Comparison of misclassification error rate for different scenarios using SVM classifier.

DOI: http://dx.doi.org/10.25098/5.2.16

The Scientific Journal of Cihan University – Sulaimaniya **PP: 10-29**
Volume (5), Issue (2), December 2021
ISSN 2520-7377 (Online), ISSN 2520-5102 (Print)

Finally, the performance of the proposed fusion system was compared with some existing state-of-the-art systems as shown in Table 5. The proposed system provides a promising result especially in terms of overall classification accuracy when comparing to the existing methods, which was due to the integration of CL, GWT and LGIP methods. However, in the other researches a huge number of features were used, while in the proposed system, 137 features were used with the best performance results achieved.

Table 5. Comparison of proposed classification accuracy with recent techniques

Author	Year	COVID datasets		Accuracy (%)
		Method	Classifier	
Zulfaezal et al. [21]	2020	CNN (ResNet101)	----	71.90
Elaziz et al. [24]	2020	FrMEMs	KNN	96.09
Bourouis et al. [19]	2021	SSDDMM	Bayes	93.03
Ohata et al. [20]	2021	CNN	MLP	95.64
Keidar et al. [23]	2021		DNNS	90.30
Proposed work		CT, GWT, and LGIP	SVM	**96.18**

From the above experimental results, it is obvious that the proposed framework can be successfully applied to more precisely identify COVID-19 cases from CXR images. As a result, this can help doctors to do a clear diagnosis, or it can be used as a tool to provide second opinion in identifying COVID-19 cases.

5. Conclusion:

Early diagnosis of COVID-19 patients is essential in preventing the disease from spreading. Image processing approaches utilized to X-ray images can help identify COVID-19 by employing artificial intelligence. This work designed an intelligent method for the COVID-19 identification using feature fusion and machine learning model. Each trained model was assessed using benchmark performance metrics e.g. accuracy, precision, sensitivity, F1-score, and misclassification error rate under seven different scenarios concerned with balanced learning and classification approach. In order to test the proposed model, a publicly available CXR images was used, the same dataset was used in earlier COVID-19 studies. The proposed feature fusion pipeline showed a higher overall classification accuracy (96.18 ± 0.43 %) than the accuracies achieved by using features attained by individual feature extraction methods, such as CT, GWT and LGIP. In addition, experimental results revealed that the proposed model is more effective than previous works carried out for the detection of COVID-19 using CXR imaging.

DOI: http://dx.doi.org/10.25098/5.2.16

References:

[1] Pham TD. Classification of COVID-19 chest X-rays with deep learning: new models or fine tuning? Heal Inf Sci Syst 2021;9. https://doi.org/10.1007/s13755-020-00135-3.

[2] Rahman T, Khandakar A, Qiblawey Y, Tahir A, Kiranyaz S. Since January 2020 Elsevier has created a COVID-19 resource centre with free information in English and Mandarin on the novel coronavirus COVID- 19 . The COVID-19 resource centre is hosted on Elsevier Connect , the company ' s public news and information 2020.

[3] Wang D, Hu B, Hu C, Zhu F, Liu X, Zhang J, et al. Clinical Characteristics of 138 Hospitalized Patients with 2019 Novel Coronavirus-Infected Pneumonia in Wuhan, China. JAMA - J Am Med Assoc 2020;323:1061–9. https://doi.org/10.1001/jama.2020.1585.

[4] Apostolopoulos ID, Mpesiana TA. Covid-19: automatic detection from X-ray images utilizing transfer learning with convolutional neural networks. Phys Eng Sci Med 2020;43:635–40. https://doi.org/10.1007/s13246-020-00865-4.

[5] Abbas A, Abdelsamea MM, Gaber MM. Classification of COVID-19 in chest X-ray images using DeTraC deep convolutional neural network. Appl Intell 2021;51:854–64. https://doi.org/10.1007/s10489-020-01829-7.

[6] Aradhya VNM, Mahmud M, Guru DS, Agarwal B, Kaiser MS. One-shot Cluster-Based Approach for the Detection of COVID–19 from Chest X–ray Images. Cognit Comput 2021;13:873–81. https://doi.org/10.1007/s12559-020-09774-w.

[7] Narin A, Kaya C, Pamuk Z. Automatic Detection of Coronavirus Disease (COVID-19) Using X-ray Images and Deep Convolutional Neural Networks. 2020.

[8] Ahmad F, Farooq A, Ghani MU. Deep Ensemble Model for Classification of Novel Coronavirus in Chest X-Ray Images. Comput Intell Neurosci 2021;2021. https://doi.org/10.1155/2021/8890226.

[9] Turkoglu M. COVIDetectioNet: COVID-19 diagnosis system based on X-ray images using features selected from pre-learned deep features ensemble. Appl Intell 2021;51:1213–26. https://doi.org/10.1007/s10489-020-01888-w.

[10] Al-Waisy AS, Mohammed MA, Al-Fahdawi S, Maashi MS, Garcia-Zapirain B, Abdulkareem KH, et al. COVID-DeepNet: Hybrid Multimodal Deep Learning System for Improving COVID-19 Pneumonia Detection in Chest X-ray Images. Comput Mater Contin 2021;67:2409–29. https://doi.org/10.32604/cmc.2021.012955.

[11] Punn NS, Agarwal S. Automated diagnosis of COVID-19 with limited posteroanterior chest X-ray images using fine-tuned deep neural networks. Appl Intell 2021;51:2689–702. https://doi.org/10.1007/s10489-020-01900-3.

[12] Zargari Khuzani A, Heidari M, Shariati SA. COVID-Classifier: an automated machine learning model to assist in the diagnosis of COVID-19 infection in chest X-ray images. Sci Rep 2021;11:1–6. https://doi.org/10.1038/s41598-021-88807-2.

[13] López-Cabrera JD, Orozco-Morales R, Portal-Diaz JA, Lovelle-Enríquez O, Pérez-Díaz M. Current limitations to identify COVID-19 using artificial intelligence with chest X-ray imaging. Health Technol (Berl) 2021;11:411–24. https://doi.org/10.1007/s12553-021-00520-2.

DOI: http://dx.doi.org/10.25098/5.2.16

[14] Narin A, Kaya C, Pamuk Z. Automatic detection of coronavirus disease (COVID-19) using X-ray images and deep convolutional neural networks. Pattern Anal Appl 2021;24:1207–20. https://doi.org/10.1007/s10044-021-00984-y.

[15] Singh AK, Kumar A, Mahmud M, Kaiser MS, Kishore A. COVID-19 Infection Detection from Chest X-Ray Images Using Hybrid Social Group Optimization and Support Vector Classifier. Cognit Comput 2021. https://doi.org/10.1007/s12559-021-09848-3.

[16] Jain R, Gupta M, Taneja S, Hemanth DJ. Deep learning based detection and analysis of COVID-19 on chest X-ray images 2020.

[17] Karthik R, Menaka R, Hariharan M. Learning distinctive filters for COVID-19 detection from chest X-ray using shuffled residual CNN. Appl Soft Comput 2021;99:106744. https://doi.org/10.1016/j.asoc.2020.106744.

[18] Nur-a-alam, Ahsan M, Based MA, Haider J, Kowalski M. COVID-19 detection from chest X-ray images using feature fusion and deep learning. Sensors 2021;21:1–30. https://doi.org/10.3390/s21041480.

[19] Bourouis S, Alharbi A, Bouguila N. Bayesian Learning of Shifted-Scaled Dirichlet Mixture Models and Its Application to Early COVID-19 Detection in Chest X-ray Images. J Imaging 2021;7:7. https://doi.org/10.3390/jimaging7010007.

[20] Ohata EF, Bezerra GM, Victor J, Vieira A, Neto L, Albuquerque B, et al. Automatic Detection of COVID-19 Infection Using Chest X-Ray Images Through Transfer Learning 2021;8. https://doi.org/10.1109/JAS.2020.1003393.

[21] Zulfaezal M, Azemin C, Hassan R, Izzuddin M, Tamrin M, Ali MA. COVID-19 Deep Learning Prediction Model Using Publicly Available Radiologist-Adjudicated Chest X-Ray Images as Training Data : Preliminary Findings 2020;2020.

[22] Sethy PK, Behera SK, Ratha PK, Biswas P. Detection of coronavirus disease (COVID-19) based on deep features and support vector machine. Int J Math Eng Manag Sci 2020;5:643–51. https://doi.org/10.33889/IJMEMS.2020.5.4.052.

[23] Keidar D, Yaron D, Goldstein E, Shachar Y, Blass A, Charbinsky L, et al. COVID-19 classification of X-ray images using deep neural networks. Eur Radiol 2021. https://doi.org/10.1007/s00330-021-08050-1.

[24] Elaziz MA, Hosny KM, Salah A, Darwish MM, Lu S, Sahlol AT. New machine learning method for imagebased diagnosis of COVID-19. PLoS One 2020;15:1–13. https://doi.org/10.1371/journal.pone.0235187.

[25] Rasheed J, Hameed AA, Djeddi C, Jamil A, Al-Turjman F. A machine learning-based framework for diagnosis of COVID-19 from chest X-ray images. Interdiscip Sci Comput Life Sci 2021;13:103–17. https://doi.org/10.1007/s12539-020-00403-6.

[26] Hira S, Bai A, Hira S. An automatic approach based on CNN architecture to detect Covid-19 disease from chest X-ray images. Appl Intell 2021;51:2864–89. https://doi.org/10.1007/s10489-020-02010-w.

[27] Al-antari MA, Hua CH, Bang J, Lee S. "Fast deep learning computer-aided diagnosis of COVID-19 based on digital chest x-ray images." Appl Intell 2021;51:2890–907. https://doi.org/10.1007/s10489-020-02076-6.

DOI: http://dx.doi.org/10.25098/5.2.16

[28] Afifi A, Hafsa NE, Ali MAS, Alhumam A, Alsalman S. An ensemble of global and local-attention based convolutional neural networks for COVID-19 diagnosis on chest X-ray images. Symmetry (Basel) 2021;13:1–25. https://doi.org/10.3390/sym13010113.

[29] Chowdhury MEH, Rahman T, Khandakar A, Mazhar R, Kadir MA, Mahbub ZB, et al. Can AI Help in Screening Viral and COVID-19 Pneumonia? IEEE Access 2020;8:132665–76. https://doi.org/10.1109/ACCESS.2020.3010287.

[30] Rahman T, Khandakar A, Qiblawey Y, Tahir A, Kiranyaz S, Abul Kashem S Bin, et al. Exploring the effect of image enhancement techniques on COVID-19 detection using chest X-ray images. Comput Biol Med 2021;132:104319. https://doi.org/https://doi.org/10.1016/j.compbiomed.2021.104319.

[31] Wady SH, Yousif RZ, Hasan HR. A Novel Intelligent System for Brain Tumor Diagnosis Based on a Composite Neutrosophic-Slantlet Transform Domain for Statistical Texture Feature Extraction. Biomed Res Int 2020;2020:8125392. https://doi.org/10.1155/2020/8125392.

[32] Candès E, Demanet L, Donoho D, Ying L. Fast Discrete Curvelet Transforms. SIAM J Multiscale Model Simul 2006;5. https://doi.org/10.1137/05064182X.

[33] Hashim A. Image Denoising Based Improved Curvelet Threshold 2021.

[34] Lahmiri S, Boukadoum M. Hybrid discrete wavelet transform and Gabor filter banks processing for mammogram features extraction. 2011 IEEE 9th Int New Circuits Syst Conf NEWCAS 2011 2011;2013:53–6. https://doi.org/10.1109/NEWCAS.2011.5981217.

[35] Zhou L, Wang H. Local gradient increasing pattern for facial expression recognition. Proc. - Int. Conf. Image Process. ICIP, 2012, p. 2601–4. https://doi.org/10.1109/ICIP.2012.6467431.

[36] Lubing Z, Han W. Local gradient increasing pattern for facial expression recognition. 2012. https://doi.org/10.1109/ICIP.2012.6467431.

[37] Ahmed S. Ethnicity Identification based on Fusion Strategy of Local and Global Features Extraction. International Journal of Multidisciplinary and Current Research, Vol. 4, 2016, No 2, pp. 200-205.

DOI: http://dx.doi.org/10.25098/5.2.16